WESLEYAN UNIVERSITY

VORTEX ACTIVATION IN SUPERFLUID FILMS

by

Seungwook Ma

A Thesis submitted to the Faculty
of Wesleyan University in partial fulfillment of
the requirements for the degree of Master of Arts

Middletown, Connecticut May 1999

Table of Contents

I. Introduction

1.1 The Experiment 3
1.2 The Wave 4
1.3 The Splitting 7
1.4 The Circulation 9
1.5 The Wave Velocity 16
1.6 Thermal Activation 18
1.7 Summary 19

II. The Model

2.1 Small Oscillations 21
2.2 β-Shift 23
2.3 Doppler Shift 26
2.4 Iterate Me 29

III. The Data

3.1 The Preparation 32
3.2 Qualitative Features 34
3.3 The Numbers 41

IV. Conclusion

Appendix

A. The Equations of Motion 45
B. The Explicit Model 49

Bibliography

I

Introduction

High amplitude, third sound waves are found to accelerate and decelerate circular flow states in thin films of superfluid helium. The observed swirling action is a quantum mechanical feature. In our experimental cell, circular flow depends upon a distribution of quantized elements of circulation, called vortices. In order to change the circulation, the distribution must be permanently rearranged. Ordinarily, vortices are pinned by the roughness of the substrate surface. However, the sloshing of the third sound wave may displace vortices. Experimentally, we find that swirling depends upon the wave amplitude and the temperature. In this thesis, we introduce the swirling mechanism as a flow assisted thermal activation of pinned vortices.

Third sound is a wave mode that travels through thin films of superfluid helium. They are similar to long wavelength gravity waves and can be analogous to tidal motion. Our film thickness ranges from three to twenty atomic layers. In this microscopic regime, gravity is negligible and the van der Waals acts as the primary restoring force. The third sound wave is remarkably well described by classical hydrodynamics. The macroscopic equations of motion are identical to that of a non-viscous classical fluid.

In the lab, we study traveling waves on the inner surfaces of a circular cavity about the size of a dime. The relevant dynamics include a superposition of the third sound wave and a background circulation. The wave may be visualized by holding a bowl of water and agitating it in a small circular motion. The background circulation is a

uniform rotational motion of the fluid. Notably, at low temperatures, the wave dissipates energy, but the circulation persists.

The circulation we encounter in the lab cannot be derived from classical physics. In bulk helium, the circulation is quantized as vortices. A vortex is a singularity in the flow field, analogous to water swirling around a drain. Unlike their classical counterparts, our vortices persist on timescales much longer than the length of our experiments. Although no direct experimental evidence demonstates the existence of quantized vortices in thin films of helium, a distribution of vortices can gives rise to the experimentally observed flow fields.

In addition to the circulation, energy dissipation of the third sound wave results from vortices. In superfluid films, energy dissipation has traditionally been linked to thermo-mechanical effects. Temperature oscillations, associated with the wave agitation, give rise to imperfect thermal exchange between the fluid and the substrate surface, between the fluid and the surrounding vapor and within the fluid itself. Current models have not been correctly able to account for the unexpectedly large dissipation associated with the third sound wave. In our model, damping results from frictional losses as vortices are dragged across the substrate surface.

Damping of the third sound wave is intimately related to the circulation. In order to change the circulation, vortices must be permanently moved. To move a vortex, work must be done against frictional contact with the substrate surface. The energy required to move vortices emerges as an acceleration or deceleration of the flow. There is an unambiguous relationship among the energy transfer, the change in the circulation and the rearrangement of vortices.

The motion of vortices, as both a hydrodynamic and topological problem, is subtle and not well understood. Our model circumvents these shortcomings by considering only the energetic aspect of the physical system. At any point in the cell, the wave velocity oscillates back and forth. If the forward wave dissipates more energy

than the reverse wave, the wave will increase the circulation. By symmetry, the converse also holds. Swirling results from asymmetric dissipation of the forward and reverse wave flows.

Generally, vortices are pinned to imperfections in the substrate surface. The fluid is relatively shallow over a bump. Less fluid associated with the vortex flow field corresponds to a lower energy state. Vortices are trapped in these potential wells. The number of free vortices is associated with thermal activation. As the temperature or the external flow increases, de-pinning is increasingly probable. In our model, only free vortices may affect the circulation. Consequently, swirling is considered a flow assisted thermal activation of an existing reservoir of pinned vortices.

1.1 Experiment

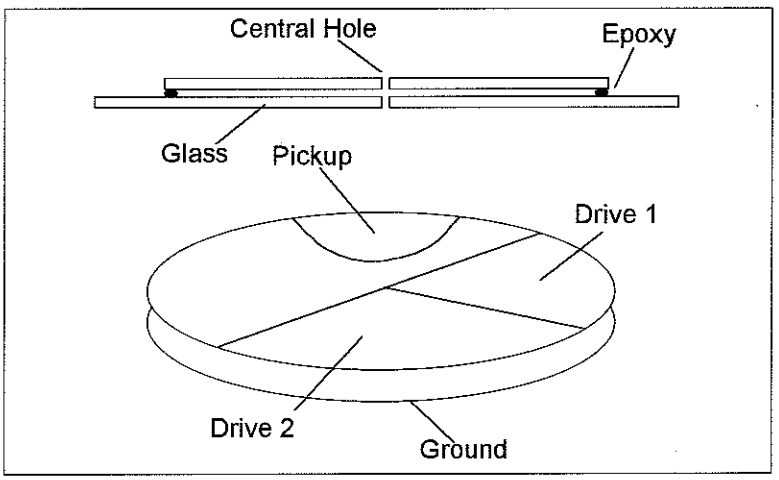

Figure 1.1

In our experimental setup, liquid helium is adsorbed onto the inner surfaces of a small hollow disk. At our film thickness, the van der Waals attraction to the surrounding surfaces dominates. Since superfluid has no viscosity, it spreads to cover all surfaces equally. At the center are two small holes through which helium enters the cell. Notably, in our analysis, we discount the presence of the holes, a complication that

is relatively small. Above and below the disk are a series of capacitor plates: two drive plates and one pickup plate. Since helium is a weak dielectric, we can oscillate the film by applying an oscillatory voltage to the two drive plates. In addition, we can determine the amplitude and frequency of our third sound wave by measuring the change in capacitance at the pickup plate. Notably, the third sound frequency is twice the drive frequency because the force on a dielectric is related to the square of the electric field. In order to collect the data, we step through drive frequency and measure the resulting wave amplitude.

1.2 The Wave

At low amplitudes, the third sound waves are Bessel functions. These solutions are consistent with the experimental values for the resonant frequencies of the normal modes. In order to derive the wave solutions, we assume an incompressible, classical fluid, without viscosity and in the long wavelength limit. Typically, the wavelength is millions of times greater than the film thickness. In this limiting case, there is no significant vertical acceleration. Height oscillations are due only to motion parallel to the substrate surface. They are a consequence of incompressibility. The equations of motion are given by the following.

$$\frac{\partial\langle\vec{v}\rangle}{\partial t} = -g\vec{\nabla}\eta$$
$$\frac{\partial\eta}{\partial t} = h_0\vec{\nabla}\cdot\langle\vec{v}\rangle \qquad (1.1), (1.2)$$

The first equation is a linearized form of Euler's equation and is analogous to Newton's second law. The second equation is a statement of incompressibility. η is the fluid's

vertical deviation from the average height. The triangular brackets indicate an average over the film thickness, defined as follows.

$$\langle v_x \rangle = \frac{1}{h_0} \int_0^{h_0} \frac{\partial v_x}{\partial z} dz \qquad (1.3)$$

In the long wavelength limit, we discount the vertical component of the fluid velocity. The derivation of these equations is given in appendix A.

Fundamental Constants	
c_3	third sound speed
h_0	average fluid height
g	characteristic van der Waals strength
a	experimental cell radius
ρ	fluid density
m_{He4}	mass of helium-4 atom
k	wave number
$x_{m,n}$	n^{th} zero derivative for m^{th} Bessel function

Table 1.1

If we assume oscillatory solutions, we may solve by a separation of variables. Elimination of v from equations (1.1) and (1.2) gives rise to the wave equation.

$$\nabla^2 \eta + k^2 \eta = 0 \qquad (1.4)$$

In cylindrical coordinates, the radial solutions are Bessel functions. The oscillation frequencies are governed by the boundary conditions. The radial velocity must be zero at the rim (r=a). Because of the driving mechanism, we can only excite modes that are symmetric across the top and bottom of the cell. Symmetry does not permit a non-zero radial flow at the rim.

$$\omega_{m,n} = c_3 k_{m,n} = \sqrt{g h_0}\,\frac{x_{m,n}}{a} \qquad (1.5)$$

Here, $k_{m,n}$ is the wave number, c_3 is the speed of sound through the fluid, and $x_{m,n}$ are the arguments for n^{th} zero derivative of the m^{th} order Bessel function.

$$c_3 = \sqrt{g h_0}$$
$$k = \frac{x_{m,n}}{a} \qquad (1.6), (1.7)$$

The resulting wave modes are given as follows.

$$\eta = \eta_{m,n} J_m(kr)\cdot e^{i(m\phi-\omega t)}$$
$$v_r = \eta_{m,n}\frac{c_3 a}{x_{m,n} h_0}\frac{\partial}{\partial r} J_m(kr)\cdot e^{i(m\phi-\omega t)} \qquad (1.8), (1.9), (1.10)$$
$$v_\phi = i\eta_{m,n}\frac{c_3 a}{x_{m,n} h_0}\frac{m}{r} J_m(kr)\cdot e^{i(m\phi-\omega t)}$$

When we drive the fluid, all of the modes are activated. However, near resonance, we can assume that only one mode is present. This assumption is valid, because the experimental, resonant frequencies are well correlated to single dominant modes. Modes on resonance are Q (10000-500000) times larger than those off

resonance. The current paper focuses on circularly polarized, traveling wave solutions for the (2,1) mode. A snapshot of the wave is given by figure 1.2. Without a circulation, the time evolution can be visualized by rotating the figure about the central axis.

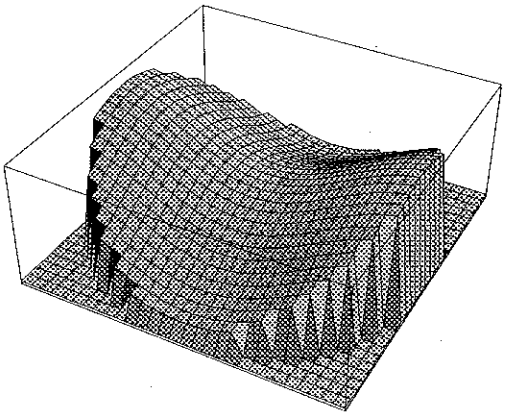

Figure 1.2

1.3 The Splitting

At low amplitudes, the resonance responds like a damped mass on a spring. In our cell, there are actually two modes with the same frequency. The two modes correspond to clockwise and counterclockwise waves. For a perfectly round cell, the clockwise and counterclockwise waves are identical. Given a background circulation, one wave will travel faster than the other.

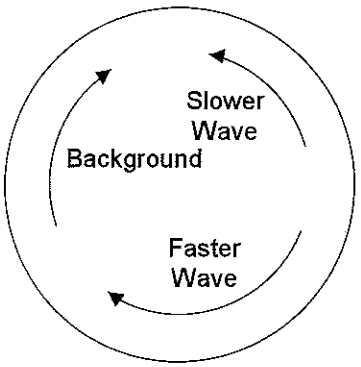

Figure 1.3. Third sound waves in a circular cell.

Each wave will experience an equal and opposite Doppler shift.

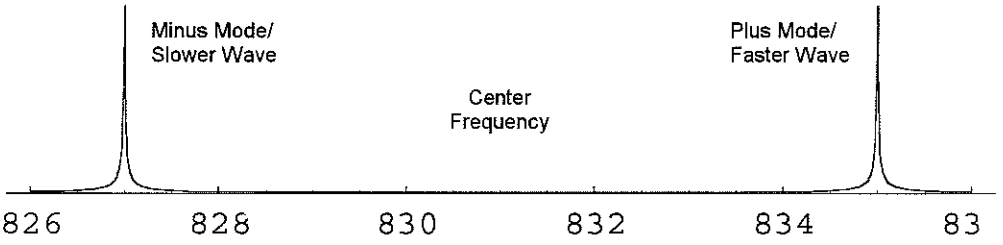

Figure 1.4. Frequency splitting from a Doppler shift.

For a one-dimensional plane wave, the frequency splitting is equal to the background flow.

$$\frac{f_{resonant} - f_{center}}{f_{center}} = \pm \frac{v_{background}}{c_3} \qquad (1.11)$$

In a circular cell, the circulation is a function of the radius. The measured, frequency splitting is a weighted average over the entire flow field.

$$\frac{f_{resonant} - f_{center}}{f_{center}} = \pm \gamma_{m,n} \frac{v_{background}(r_0)}{c_3} \qquad (1.12)$$

The weighting factor, $\gamma_{m,n}$, relates the size of the frequency splitting to the circulation at some convenient (and arbitrary) radial location, r_0. The factor depends only on the given mode. Qualitative features of the circulation are independent of the size of the splitting. The relationship of the frequency splitting to the underlying flow field is given rigorous treatment in both Hai's and Crista's dissertations. To avoid redundancy, only the final result, equation (1.13), is presented,

$$\gamma_{m,n} = \frac{c_3}{v_b(r_0)} \frac{2m}{(x_{m,n}^{\ 2} - m^2) J_m^{\ 2}(x_{m,n})} \int_0^{x_{m,n}} v_b(x) J_m^{\ 2}(x) - \frac{J_m'(x) J_m(x)}{x} \frac{d}{dx}(x \cdot v_b(x)) dx \tag{1.13}$$

where, x is the scaled radial coordinate defined as

$$x = \frac{x_{m,n}}{a} r \tag{1.14}$$

Both Crista and Hai set r_0=a. The weighting factor depends upon the choice of r_0. Presently, r_0 is an adjustable parameter.

In theory, if we have the frequency splitting for all the modes (there are infinitely many), we can know the exact radial dependence of the circulation. Our understanding is limited by the fact that we can excite only a few modes.

1.4 The Circulation

$$\kappa \equiv \oint_C \vec{v}_s \cdot d\vec{l}$$

If a classical fluid is incompressible and subject to conservative forces, the circulation is a constant of time (Kelvin's circulation theorem). Our fluid does not exhibit viscosity and only responds to the gradient of the pressure, the van der Waals' attraction and the electrostatic driving force. Classically, we cannot create a circulation. In the previous section, we uncovered a circulation from the frequency splitting. This phenomenon is a quantum mechanical feature that requires the introduction of vortices.

There are numerous speculations on the formation of vortices. They may be generated by the turbulence of boiling as helium is cooled through the superfluid transition temperature. Vortex-anti-vortex pairs may occur spontaneously by thermal activation, analogous to pair production of electrons and positrons at high temperatures. Although a vortex costs an enormous amount of energy, they may persist at extremely low temperatures. Our experiments run at tenths of a Kelvin. Because of pinning, they do not have the opportunity to find one another quickly and annihilate.

Vortices are the circulation quanta. For a superfluid, the velocity is quantized. Let's derive the quantization conditions and see how a distribution of vortices can give rise to a circulation. Start with a uniform quantum fluid. The probability of finding any bit of fluid is constant.

$$probability = |\Psi|^2 = \Psi_0^{\,2} \qquad (1.15)$$

From this assertion, the wave function is known to within a phase factor.

$$\Psi = \Psi_0 e^{-i\Phi(\vec{r})} \tag{1.16}$$

In a small element of fluid, dV, the expectation value of the momentum is given by the following.

$$\left\langle \vec{p} \right\rangle = \frac{\left\langle \Psi \left| \frac{\hbar}{i} \nabla \right| \Psi \right\rangle}{\left\langle \Psi \mid \Psi \right\rangle} \cong \hbar \nabla \Phi(\vec{r}) \tag{1.17}$$

The momentum is simply $m_{He4}v_s$.

$$\vec{v}_s = \frac{\hbar}{m_{He4}} \nabla \Phi(\vec{r}) \tag{1.18}$$

Take the integral of each side over a closed path.

$$\begin{aligned} \oint \vec{v}_s d\vec{l} &= \frac{\hbar}{m_{He4}} \oint \nabla \Phi(\vec{r}) d\vec{l} \\ &= \frac{\hbar}{m_{He4}} \left(\Phi_{start} - \Phi_{end} \right) \\ &= \frac{\hbar}{m_{He4}} \Delta \Phi \end{aligned} \tag{1.19}$$

Around any closed loop, the phase change must be an integral multiple of 2π. Therefore, we may define the circulation quantization as follows.

$$\oint \vec{v}_s d\vec{l} = 2\pi \frac{\hbar}{m_{He4}} N \qquad (1.20)$$

From Kelvin's circulation theorem, the fluid is curl-free everywhere except at points for which the velocity is undefined. These points are vortices.

We can directly integrate equation (1.20) over a circular path and calculate the flow field for a single vortex at the origin.

$$\vec{v}_s(r) = \frac{\hbar}{m_{He4}} \frac{1}{r} \hat{\phi} \qquad (1.21)$$

From the flow field, we can calculate the energy of a vortex.

$$E = \int \frac{1}{2} v^2 dm = \pi\rho \left(\frac{\hbar}{m_{He4}} \right)^2 Ln\left(\frac{b}{a} \right)$$
$$b \cong \sqrt{\frac{1}{n}} \qquad (1.22)$$

Here, a ($\cong 1$ *angstrom*) is the vortex core size, b is a characterisic distance between neighboring vortices and n is the number of vortices per unit area. With a circulation and no pinning, there are about 10^4 vortices per square centimeter. With pinning, the number may be as large as 10^{11} vortices per square centimeter.

A collection of vortices within a closed path gives rise to a circulation.

$$v_{background}(r) = \frac{\hbar}{m_{He4}} \frac{1}{r} N_{enclosed}(r) \qquad (1.23)$$

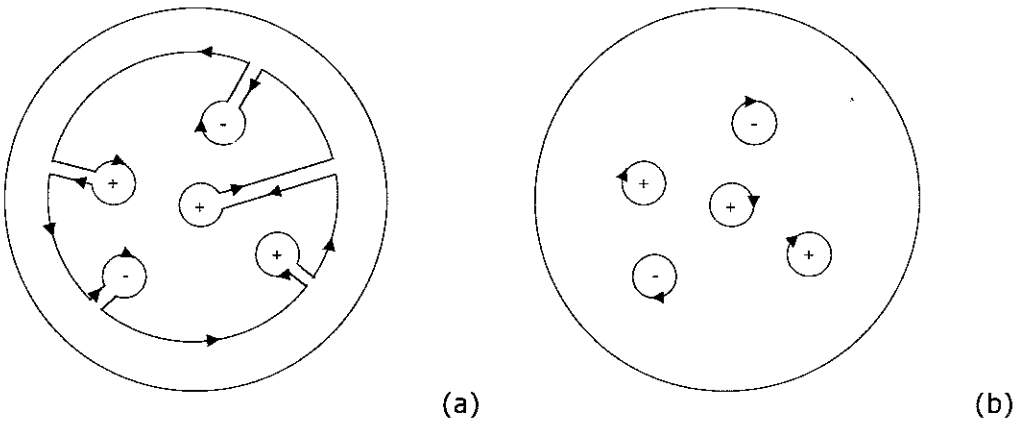

Figure 1.5. A path integral over the velocity field may be broken into two steps. The result is the sum of steps (a) and (b). (a) Since vortices are excluded, the integral is zero. (b) The integral depends only on the number of enclosed vortices

Equation (1.23) relates the background circulation to a distribution of vortices. An integral of the velocity field over a closed path depends only on the number of enclosed vortices. If vortices are excluded, the integral is zero.

To understand how vortices may create or alter the circulation, consider two limiting cases. Assume a uniform distribution of vortices such that along every concentric circular path there is an equal number of positive and negative vortices. In this case, the circulation is zero. Now, move all of the positive vortices to the center and all of the negative vortices to the outer rim. Every concentric circular path, for which $r<a$, encloses a net number of positive vortices. The important conclusion is that radial displacement of vortices may alter the circulation. If a positive vortex is moved toward the center, the circulation increases. If it is moved toward the rim, the circulation decreases. The converse holds for negative vortices. Actually, only a small polarization of vortices is necessary to change the circulation. The effect depends upon the density of vortices. The higher the density the smaller the polarization necessary for a given change in the circulation.

The third sound sloshing may cause this polarization. Given an external flow, a vortex will experience a force according to Bernoulli's law.

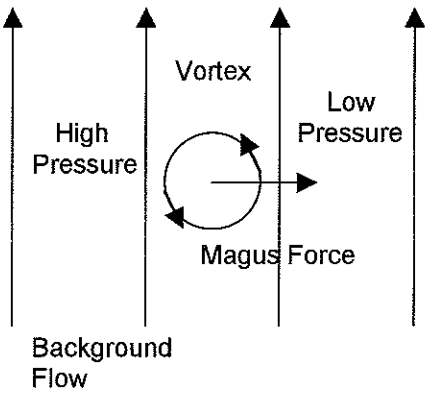

Figure 1.6. On the left side, the flows subtract. On the right side, the flows add. Higher flow corresponds to a lower pressure. Given an external flow, a vortex is subject to a Magnus force that lies along the pressure gradient.

On one side of a vortex the vortex flow and the external flow will add. On the other side, the flows will subtract. Higher flow corresponds to lower pressure. Consequently, there is a Magnus force in the direction of the pressure gradient.

$$\vec{F}_{magnus} = \rho\kappa h_0 \hat{z} \times (\vec{v}_{vortex} - \vec{v}_{external}) \qquad (1.24)$$

Moving a vortex perpendicularly to the flow requires a drag force. A vortex has no mass. Without a drag force, the vortex will move with the flow.

$$\vec{F}_{net} = F_{magnus} = \rho\kappa h_0 \hat{z} \times (\vec{v}_{vortex} - \vec{v}_{external}) = 0$$
$$\vec{v}_{vortex} = \vec{v}_{external} \qquad (1.25), (1.26)$$

If we introduce a drag force, the vortex motion has components both perpendicular and parallel to the external flow.

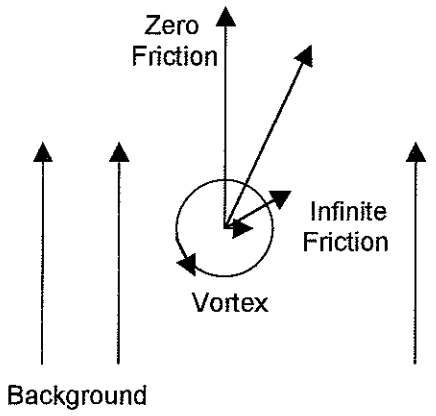

Figure 1.7. Initial vortex direction corresponding to different levels of frictional contact with the substrate surface.

$$\vec{F}_{net} = \vec{F}_{magnus} + \vec{F}_{friction} = \rho\kappa h_0 \hat{z} \times (\vec{v}_{vortex} - \vec{v}_{external}) - \gamma \vec{v}_{vortex} = 0$$

$$v_{\perp} = \frac{v_{critical}}{1 + v_{critical}^{\ 2}} v_{external}$$

$$v_{\parallel} = \frac{1}{1 + v_{critical}^{\ 2}} v_{external}$$

$$v_{critical} = \frac{\gamma}{\rho\kappa h_0}$$

(1.27), (1.28), (1.29), (1.30)

The critical velocity is the minimum external flow necessary to overcome frictional drag.

So far, our discussion is somewhat speculative. There is no way to detect directly a vortex in a superfluid film. By now, the reader should appreciate the complexity of this system. We have not even considered many other dynamics such as interactions among multiple vortices. However, we can dispense with these subtleties and consider only the energetic description. (1) To change the circulation, vortices must be moved

perpendicularly to the circulation. (2) To move a vortex, work must be done. (3) We assume that this work is proportional to both the total motion as well as the perpendicular motion. (4) Consequently, this work materializes as both a damping of the third sound wave and an acceleration or deceleration of the background circulation. These four statements may be simply stated by the following.

$$\frac{\partial \vec{v}_{background}}{\partial t} = -\left\langle RN_{free}\vec{v}_{superfluid}\right\rangle \qquad (1.31)$$

We attribute the change in the background circulation to linear damping averaged over a wave cycle. The acceleration depends upon the relative size of the forward and reverse wave velocities. The N_{free} factor is necessary because only free vortices may do work. R is a constant. In our model, there is a direct relationship between the energy dissipation and the acceleration or deceleration of the background circulation. This relationship is buried in the constant R, which is an adjustable parameter.

The Wave Velocity

In two previous sections we contradict ourselves. Equation (1.10), the azimuthal wave velocity, cannot exactly describe our system. There are two inconsistencies. If we average the wave over a cycle there is a net mass flux. Since the velocity is linear, the magnitude of the forward and reverse flows are equal. However, there is more fluid under the crests than under the troughs.

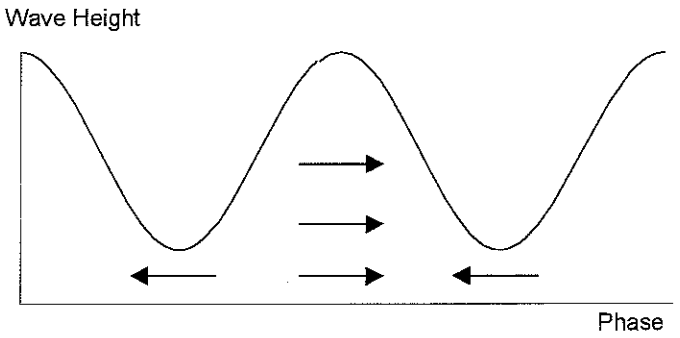

Figure 1.8. The wave height as a function of angle. For a linear wave, the magnitude of the velocity is equal under the crests as compared to the troughs. Since there is more fluid under the crests than under the troughs, a net mass of fluid moves rightward.

$$\vec{v}_{drift} = \frac{1}{h_0}\left\langle (h_0 + \eta)\cdot v_\phi \right\rangle \hat{\phi} = \frac{1}{2} c_3 \left(\frac{\eta_{m,n}}{h_0}\right)^2 \frac{m}{x_{m,n}} \frac{a}{r} J_m(x_{m,n}\frac{r}{a}) \cos(m\phi - \omega t)\hat{\phi}$$

(1.32)

The wave induces a net drift, a result that violates Kelvin's circulation theorem. Secondly, a linear wave cannot have a net effect on vortices. If the forward and reverse flows are symmetric, energy dissipation (hence vortex motion) is also symmetric, a situation that cannot swirl the film.

Although our wave solution is incorrect, the Bessel function solutions must be approximately right. If we require that the mass flux is balanced between the forward and reverse flows, we can "cook up" a new wave velocity.

$$v_{\phi,\,nonlinear} = \frac{v_\phi}{1+\eta} \qquad (1.33)$$

The above equation is a convenient manipulation of first and second order terms. Here, the reverse flow is bigger than the forward to compenste for the wave height difference.

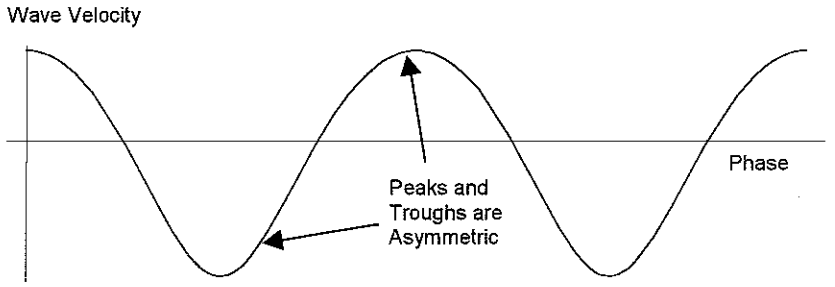

Figure 1.9. "Cooked up" wave velocity is bigger at the troughs to compensate for the wave height so that the net mass flux is zero.

Although this result is not rigorous, it matches all of physical elements that we require. A full analysis would require a solution to the nonlinear equations of motion to second order.

1.5 Thermal Activation

In the current model, we attribute the number of free vortices to thermal activation. This treatment is similar to a gas absorbed onto a two-dimensional surface. Gas molecules may be attracted to the surface in a variety of ways: electrostatic, van der Waals, etc. Regardless, the attraction corresponds to a potential well. In the simplest case, the ratio of desorbed molecules to total molecules is proportional to a Boltzman factor.

In choosing this model, our initial motivation is empirical. The article by Ellis and Wilson have demonstrate a linear relationship between a combination velocity and the log of the deceleration of the circulation.

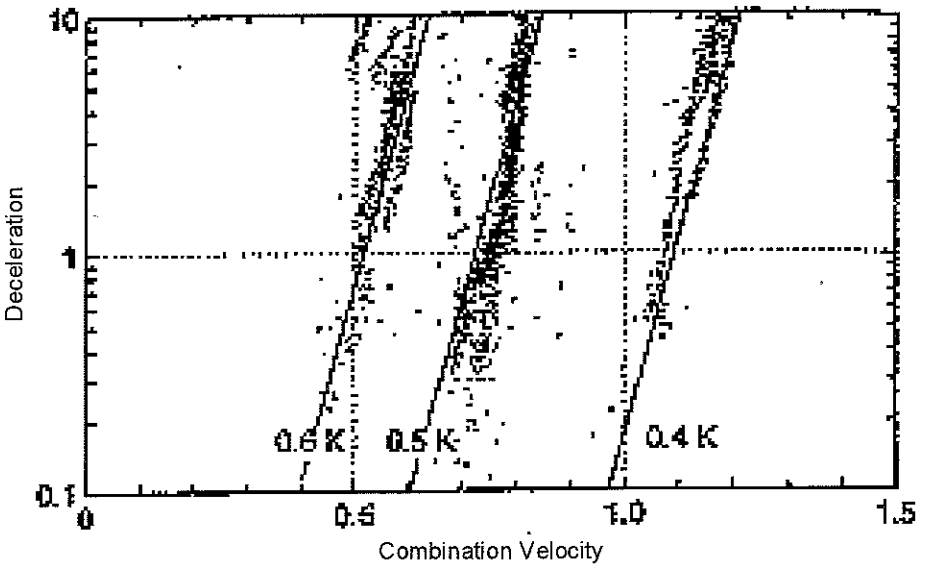

Figure 1.11

$$v_{combination} = v_{peak} + \frac{T_0}{T} v_{background} \qquad (1.34)$$

The peak velocity is the maximum wave velocity and T_0 is an adjustable parameter. Because of the inverse dependence on temperature, attributing the change in the circulation to thermal activation is appealing.

$$\frac{N_{free}}{N_0} = ge^{-\frac{\varepsilon(v_{peak}, v_{background})}{kT}} \qquad (1.35)$$

The numerator in the exponential is the pinning energy. A larger flow gives rise to a shallower potential well. As ε decreases, de-pinning a vortex becomes increasingly probably.

1.7 Summary

Although the third sound wave is remarkably well described by classical hydrodynamics, the film may be set into uniform rotational motion only by an arrangement of quantized vortices. For this reason, swirling requires net radial displacement of vortices. The specific vortex dynamics are complicated and a matter of speculation. The present model exploits the energetic description. Radial motion of vortices requires both a Magnus force and a drag force. The wave agitation generates the Magus force. We model the drag force as frictional contact between a vortex and the substrate surface. Assymetric energy dissipation by the forward and reverse wave flows gives rise to an acceleration or deceleration of the circulation. Empirical relationships suggest thermal properties. The swirling process is found to be proportional to a Boltzman factor. Generally, vortices are pinned to imperfections in the substrate surface. In the model, we attribute the de-pinning of vortices to thermal activation. The central theme of the current paper is expressed by a combination of equations (1.29) and (1.33).

$$\frac{\partial \vec{v}_{background}}{\partial t} = -\left\langle R_0 e^{-\frac{\varepsilon(v_{peak}, v_{background})}{kT}} \vec{v}_{\sup erfluid} \right\rangle \qquad (1.35)$$

II

The Model

In order to model the swirling action, we examine the third sound resonance (drive frequency v. amplitude). Particularly, we investigate the (2,1) plus mode (the faster wave). The resonance exhibits three distinct features. At low amplitudes, it resembles a damped and driven, simple harmonic oscillator. At higher amplitudes, it is modified by nonlinearity and swirling. The model mimics the manner is which the data is collected. Experimentally, we step down in drive frequency and measure the wave amplitude. The model involves an iterative procedure such that the wave amplitude and the change in the circulation are calculated for each frequency step.

2.1 Small Oscillations

For small oscillations, the steady-state amplitude may be derived from the linearized equations of motion. If we introduce a linear damping term and a periodic driving force, the equations of motion, (1.1) and (1.2), may be re-expressed as follows.

$$\frac{\partial \vec{v}}{\partial t} = -g\vec{\nabla}\eta - \gamma\vec{v} + \vec{f}_0(r,\phi)e^{-i\omega t}$$
$$\frac{\partial \eta}{\partial t} = -h_0\vec{\nabla}\cdot\vec{v} \qquad (2.1), (2.2)$$

The steady-state solution for the circular resonator is derived in Hai Luo's thesis. For the sake of clarity and to avoid redundancy, let us examine the one-dimensional case for which the driving force is uniform and sinusoidal. The solutions are planes waves, and the steady-state amplitude mimics a damped and driven, simple harmonic oscillator.

$$\frac{\eta_{m,n}}{\eta_{resoant}} = \frac{-i\gamma\omega_{resonant}}{\omega_{drive}{}^2 - \omega_{resonant}{}^2 - i\gamma\omega_{drive}} \tag{2.3}$$

The above result, equation (2.3), is identical to that of the complete solution with one exception. For a circular cell, the boundary conditions restrict the resonant frequencies to particular values. These frequencies correspond to each mode.

The equivalence of these two solutions is not unexpected.

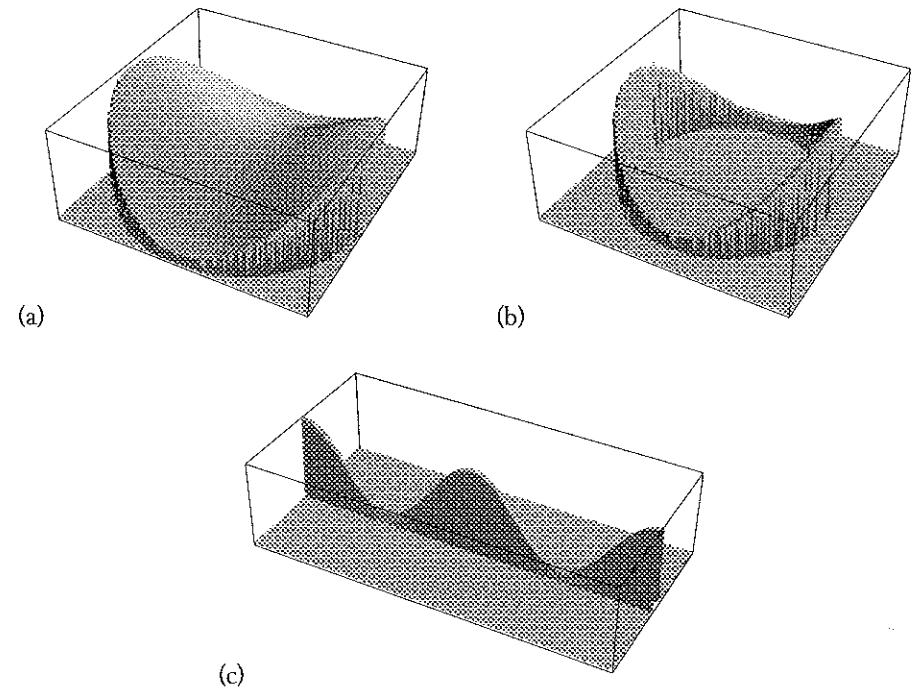

Figure 2.1. (a) Full wave solution. (b) Characteristic band. (c) Plane wave.

If we choose a characteristic radius, the resulting circular band may be unraveled to produce a plane wave. For the sake of computational efficiency, we employ the "characteristic band" approximation in the numerical analysis.

2.2 β-Shift

Our equations of motion are valid only at low amplitudes. As the amplitude increases, the resonance deviates significantly from that of the simple harmonic oscillator. From Baierlein, Ellis and Luo, frequency shifts due to nonlinearity are found to depend upon the square of the wave amplitude.

$$\frac{f_{resonance} - f_{center}}{f_{center}} = -\beta\left(\frac{\eta}{h_0}\right)^2 \qquad (2.4)$$

This result originates from both experiment and a straightforward application of classical hydrodynamics. The theory requires the presence of nonlinear terms that are excluded from our equations of motion, (2.1) and (2.2). The sign of β may we positive or negative. Its value depends upon the wave mode and the circulation. For our data, the value is roughly .016. This result is 3-4 times smaller than that from Baierlein, Ellis and Luo. The discrepancy is due to the presence of a circulation.

The β-shift comes from a coupling of the wave oscillations to a Bernoulli force. Within the fluid, variations in the fluid velocity give rise to pressure gradients according to Bernoulli's law. If a multiple a wave mode frequency is close to the Bernoulli frequency, the two frequencies will spread apart. This spreading is approximated by the β-shift.

The effect of nonlinear terms is most clearly demonstrated by comparing the linear and β-shifted resonances. At low amplitudes, the two resonances coincide. As

the wave amplitude increases, the resonant frequency shifts leftward. As the resonant frequency shifts away from the drive frequency, observed resonance is smeared leftward.

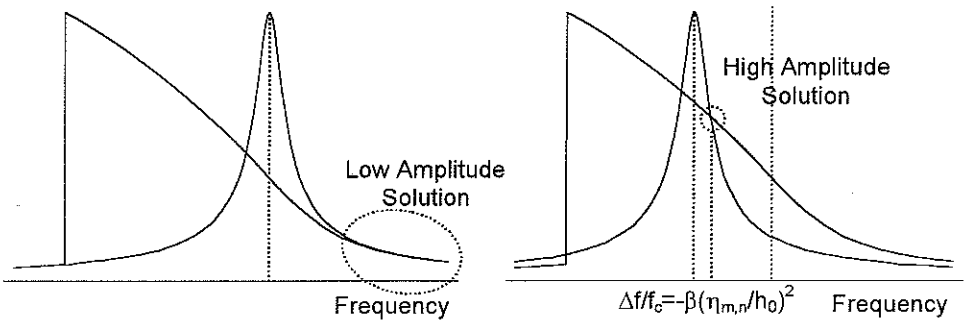

Figure 2.2. Left: At low amplitudes, the two resonaces match.. Right: At high amplitudes, the resonant frequency decreases according to the square of the amplitude.

High enough amplitude waves feature a "crash". A "crash" is a discontinuity in the resonance, characteristic of the higher drive amplitudes. We see this feature in Figure 2.5. The figure gives the β-shifted resonance for various drive amplitudes.

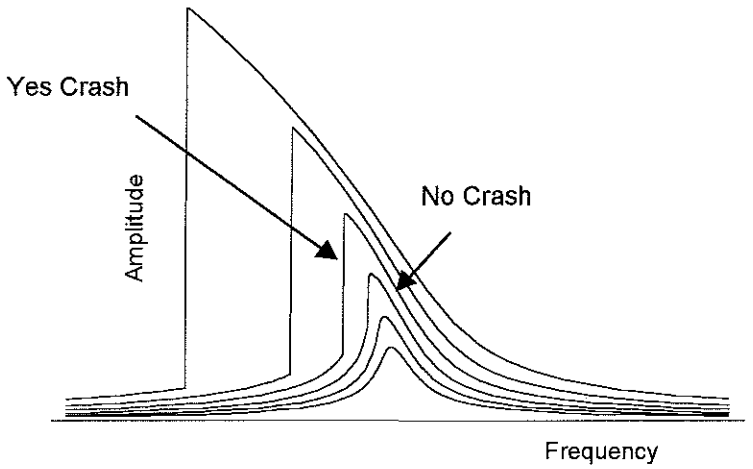

Figure 2.3. The unswirled resonance for variuos drive voltages.

The above resonances are solutions to equations (2.3) and (2.4). We approximate the steady-state amplitude by the following.

$$\eta_{m,n} = \frac{\eta_0}{\sqrt{4Q^2\left(\frac{f_{resonant} - f}{f_{center}}\right)^2 + 1}} \qquad (2.5)$$

The derivation is given in appendix B. Unlike equation (2.3), the above equation is symmetric about the peak. Graphically, the solution for the β-shifted resonance is the intersection of a sideways parabola (equation (2.4)) and a linear resonance (equation (2.5)).

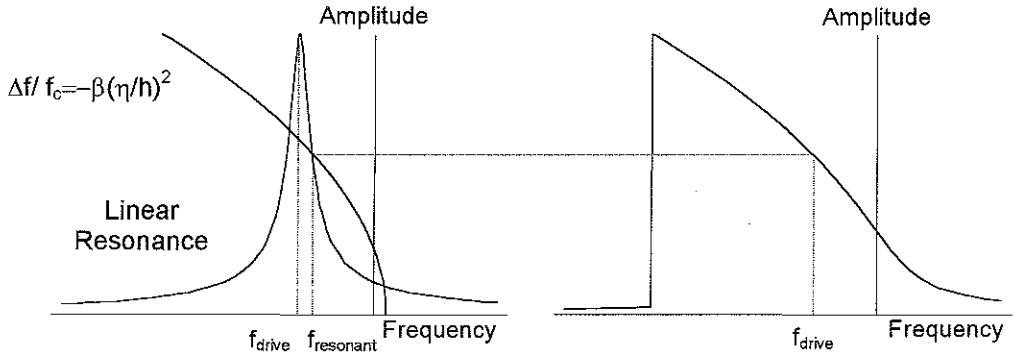

Figure 2.4. Left: Graphically solution to equations (2.3) and (2.5). Right: Observed, unswirled resonance.

Here, the center of the peak represents the drive frequency, and the intersection represents the respective resonant frequency and wave amplitude. As we sweep the linear resonance through frequency, we generate the righthand curve. At the maximum wave amplitude, there is a distinct difference between the low and high amplitude drives.

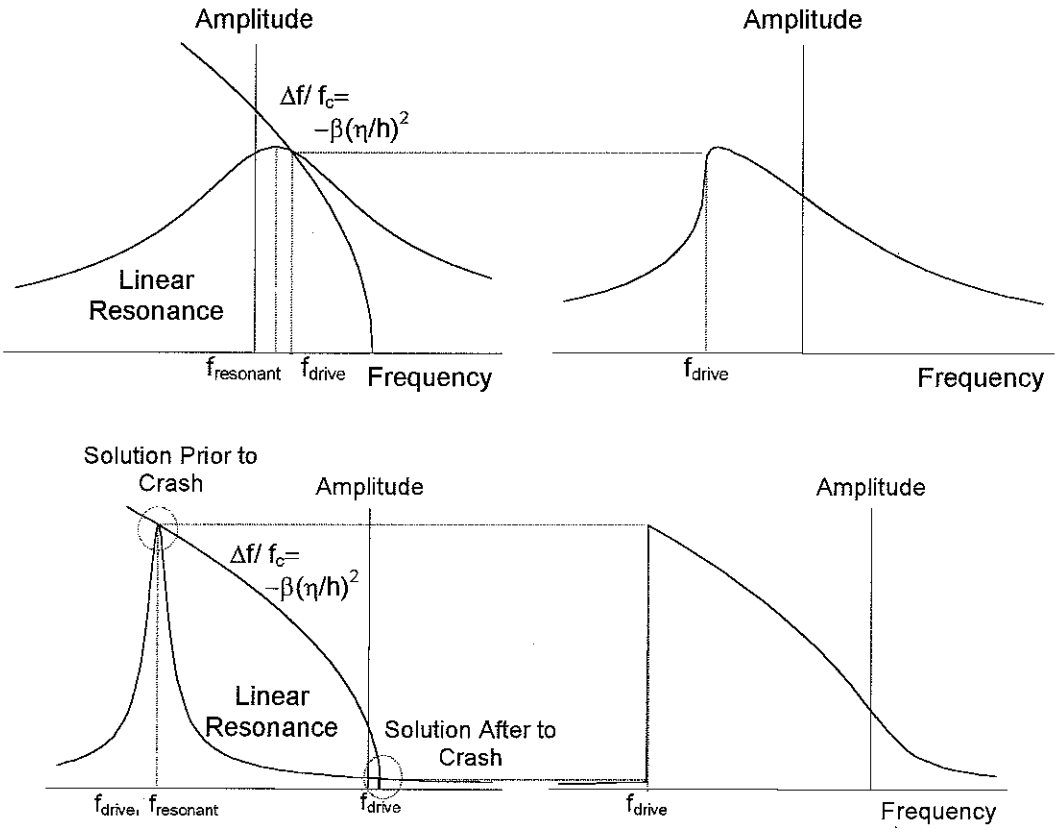

Figure 2.5. Top: Solution for low amplitude drive. Bottom: Solution for high amplitude drive.

For small drives, there is only one point of intersection. As we sweep through drive frequency, there are no discontiunities. For big drives, there are either three or one points of intersection. When the wave ampitude reaches its maximum, the solution is discontinuous. After the crash, the response is a low amplitude characterization of the tail below resonance.

2.3 Doppler Shift

Because of a Doppler effect, the frequency splitting depends upon the circulation. Consequently, the resonance must be modified, accordingly.

$$\frac{\Delta f}{f_{center}} = \gamma \frac{v(r_0)}{c_3} \tag{2.6}$$

The splitting is directly related to the circulation, because we study the up-shifted mode (the faster wave). Acceleration or deceleration of the background circulation depends upon the motion of vortices. We model the energy dissipation by vortices as frictional losses, equation (1.29).

$$a_\phi(\eta_{m,n}, v_{background}) = \frac{\partial v_{background}}{\partial t} = -R\int_0^{2\pi} v_{\sup\, erfluid,\phi} N_{free} d\theta \tag{2.7}$$

The change in the background circulation is proportional to the fluid velocity and the number of free vortices. We average over the phase of the wave because we want to extract the swirling contributions of the forward and reverse flows.

We associate the number of free vortices with thermal activation. In this framework, the number of free vortices is proportional to a Boltzman factor, equation (1.33). A simple model for the energy of a pinned vortex is the difference between the magnitude of the fluid velocity and some critical velocity. The critical velocity is the minimum external fluid velocity necessary to de-pin a vortex in the absence of thermal activation (ε=0)

$$\varepsilon = p \cdot \left(\left| v_{\sup\, erfluid} \right| - v_{critical} \right) \tag{2.8}$$

p is a constant that characterizes the pinning strength. The magnitude of the fluid velocity is the sum of the circulation and the wave velocity, equation (1.31).

$$v_{\sup\ erfluid} = v_{circulation}(r_0) + c_3 \frac{\frac{\eta_{m,n}}{h_0} J_m(\frac{x_{m,n}}{a} r_0)\cos(\theta)}{1 + \frac{\eta_{m,n}}{h_0} J_m(\frac{x_{m,n}}{a} r_0)\cos(\theta)} \qquad (2.9)$$

The phase of the wave is given by, $\theta = m\phi - \omega t$. The combination of equations (1.33), (2.6) and (2.7) model the swirling action.

$$a_\phi(\eta_{m,n}, v_{background}) = \frac{\partial v_{background}}{\partial t} = -\int_0^{2\pi} R_0 v_{\sup\ erfluid,\phi} e^{-\frac{P(|v_{\sup erfluid}| - v_{critical})}{k_{boltzman} T}} d\theta \qquad (2.10)$$

The acceleration is a function of the wave amplitude and the background circulation.

Experimentally, we find that at moderate amplitudes the circulation decreases, and at high amplitudes the circulation increases. This behavior is mimicked by equation (2.10) and shown graphically in figure (2.6).

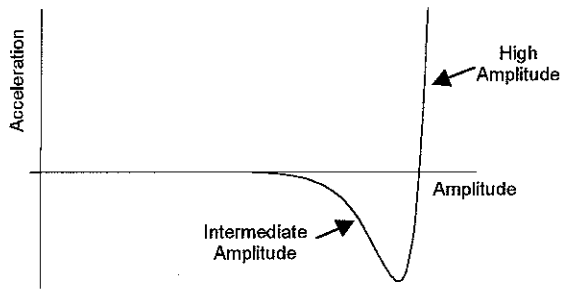

Figure 2.6. Swirling model.

Since we are concerned only with the plus mode, a decrease in the circulation corresponds to a decrease in the resonant frequency. Likewise, an increase in the circulation corresponds to an increase in the resonant frequency.

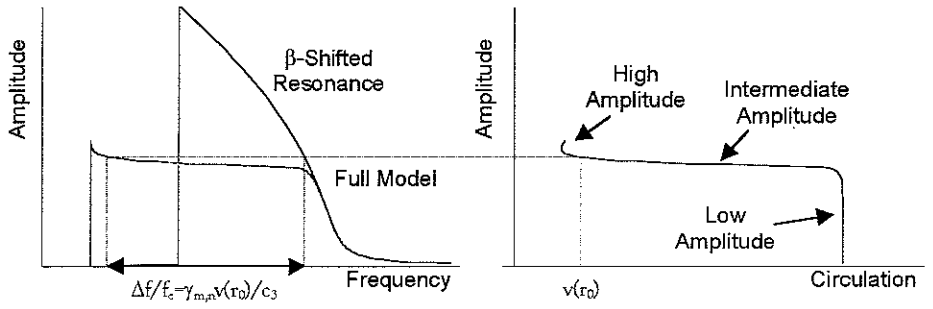

Figure 2.7. Left: β-shifted resonance v. full model. Right: Corresponding circulation at $r=r_0$.

The above figure demonstrates the swirling modification to the resonance. Similar to the β-shift, a decrease in the resonant frequency creates a leftward smearing of the resonance. Conversely, an increase in the resonant frequency causes the resonance to be compressed rightward. All in all, the horizontal difference between the two curves is proportional to the background circulation. At low amplitudes, the circulation is constant, and the two curves lie on top of one another. The wave is not large enough to activate vortices. At intermediate amplitudes, the horizontal distance grows, corresponding to a decrease in the circulation. The resonance is characterized by a sudden activation of vortices. We see a sharp bend at the start of the deceleration region. In this region, the circulation decreases because the circulation is large and the wave asymmetry is small. In the absence of pinning a dc flow will always loose energy and slow down. At the highest amplitudes, the horizontal distance decreases, corresponding to an acceleration of the circulation. Here, both the circulation is small and the wave asymmetry is big. For the azimuthal wave velocity, the back flow is always

larger than the forward flow. Consequently, the reverse flow will dissipate more energy than the forward flow. The wave will preferentially drive up the circulation.

2.4 Iterate Me

To model the resonance, we need to calculate the drive frequency versus amplitude (f_{drive} v. $\eta_{m,n}$). To mimic the experimental procedure, we step down in frequency such that:

$$f_{drive,next} = f_{drive,previous} - \frac{.001}{f_{center}}\Delta t \qquad (2.11)$$

More Constants	
Δt	experimental time step
η_0	peak amplitude of linear resonance
γ	frequency splitting weighting factor
Q	quality factor
β	strength of frequency shift due to nonlinearity

Table 2.1

We step slowly enough such that steady-state amplitude solutions are applicable. Given a known circulation and drive frequency, the wave amplitude is given by the combined solutions to the following equations.

$$\eta_{m,n} = \frac{\eta_0}{\sqrt{4Q\left(\frac{f_{resoanant} - f_{drive}}{f_{resonant}}\right)^2 + 1}}$$

$$\frac{f_{resonance} - f_{center}}{f_{center}} = \gamma \frac{v_{background}}{c_3} - \beta\left(\frac{\eta_{m,n}}{h_0}\right)^2 \qquad (2.12), (2.13)$$

The first equation is rescaled approximation to equation (2.3). The second is a combination of equations (2.4) and (2.6). Taken together, the wave amplitude is a function of the drive frequency and the background circulation.

$$\eta_{m,n} = \eta_{m,n}(f_{drive}, v_{background}) \qquad (2.14)$$

The wave amplitude and circulation may then be used to calculate the acceleration of the background circulation (equation (2.7)).

$$a(\eta_{m,n}, v_{background}) = \frac{\partial v_{background}}{\partial t} = -\int_0^{2\pi} R_0 v_{\sup erfluid} e^{-\frac{P(|v_{\sup erfluid}| - v_{critical})}{k_{boltzman} T}} d\theta \qquad (2.15)$$

We linearly interpret the new circulation, such that:

$$v_{background,next} = v_{background,previous} + a(\eta_{m,n}, v_{background,previous})\Delta t \qquad (2.16)$$

With the new circulation, we repeat the above steps. All in all, this is a numerical prodecure for solving the underlying system of differential equations, a procss similar to Eulers method.

III

The Data

An analysis of the data occurs in two stages. First, we must extract physically meaningful information from the experimental apparatus. In other words, an electronic signal must be interpreted as the third sound wave frequency and amplitude. This process is well documented in the references. Presently, only a brief outline is given. The second stage involves a direct fit to the model. The data spans three temperatures and two drive amplitudes. Correct temperature and drive amplitude dependence lay strong confirmation to theory. However, certain qualitative discrepancies suggest that the vortex dynamics may be more complicated than that which is presented in the current model.

3.1 The Preparation

Two steps must be accomplished to prepare the data for our analysis. First, we need to sort through the myriad of electronics that we use to observe the third sound wave. Our observations are modified by a background signal and a phase shift. Secondly, the electronic signal must be converted into a physically relevant form. The wave height is measured from the change in capacitance at the pickup plate and recorded as a voltage.

The raw data features both translational and rotational shifts. Consequently, equation (2.3) may be re-expressed as follows.

$$\frac{\eta_{m,n}}{\eta_{resoant}} = \frac{-i\gamma\omega_{resonant}}{\omega_{drive}^{\ 2} - \omega_{resonant}^{\ 2} - i\gamma\omega_{drive}} e^{i\phi} + x_{background} + iy_{background} \qquad (3.1)$$

The rotational shift, ϕ, is due to the relative phase of the drive and pickup plates as the electronic signal passes through various filters. The translational shifts, x and y, are due to electronic cross talk as well as mechanical vibrations of the cell.

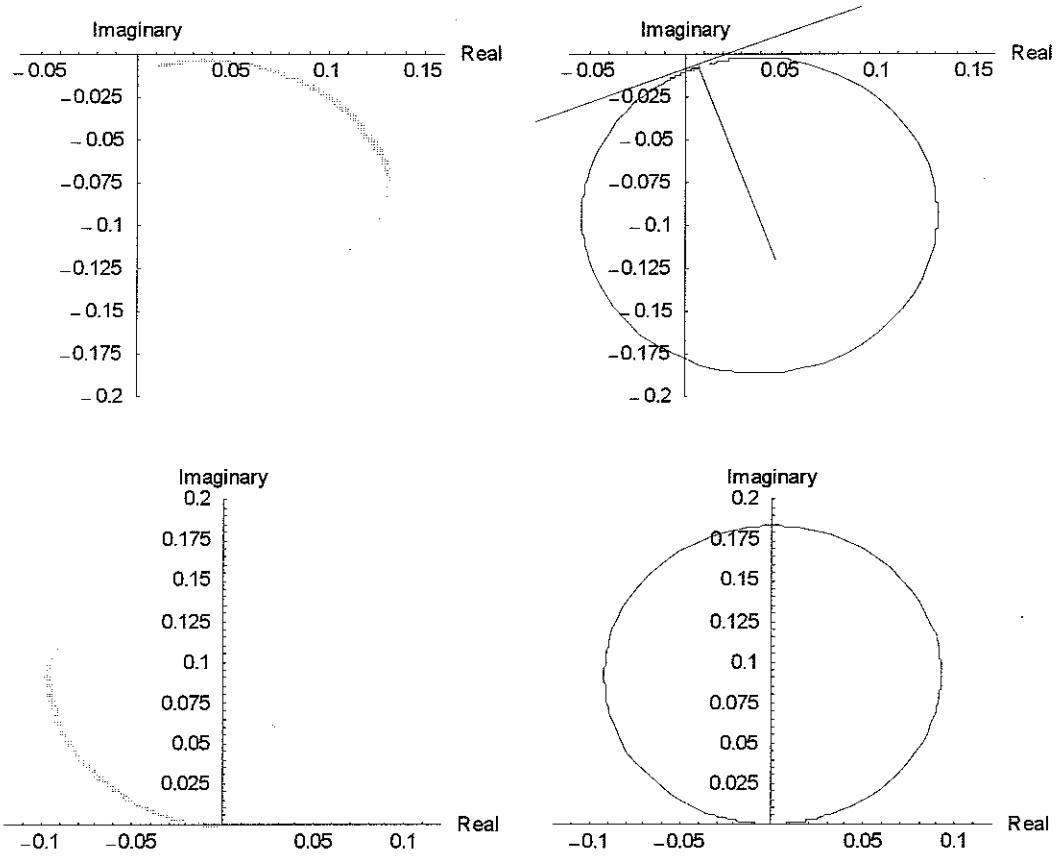

Figure 3.1 The real and imaginary components of the wave amplitude. Top: The left diagram is a plot of the raw data. The right side demonstrates the translational and rotational shifts. Bottom: Analogous plots for which the background and phase are removed.

In the complex plane, the steady-state oscillation amplitude lies on a circle. In the above figure (3.1), we may compare the raw data to the filtered data. The raw data is not only rotated but also laterally shifted. We remove the background and phase by requiring the circle to intersect the origin and by choosing clockwise as the direction of decreasing frequency. The diameter of the circle corresponds to the amplitude on resonance.

In order extract physical information, the electronic signal must be interpreted as the wave amplitude. Frequency shifts of an LCR oscillator measure the change in capacitance at the pickup plate. Consequently, we need to know both how the wave amplitude affects the oscillator frequency and how the electronics respond to frequency shifts. The former is called the sensitivity and the latter is the PLLCAL.

$$\eta_{m,n} = \frac{(signal\ voltage)}{PLLCAL \cdot sensitivity} \qquad (3.2)$$

Experimentally, the sensitivity is 115.5 Hz/nm and the PLLCAL is 250 μm/Hz. The value for $\eta_{m,n}$ is calibrated to the amplitude of the Bessel function in the equations of motion: equations (1.8), (1.9) and (1.10). For a rigorous derivation, the reader is directed to Hai Luo's thesis.

3.2 Qualitative Features

In the model, the initial conditions and the drive configuration wholly determine the shape of the resonance. Experimentally measurable parameters include the film thickness, the initial frequency splitting, the temperature and the drive voltage. Our data compares 6 different temperature (.4 K, .5 K and .6 K) and drive voltage (16.5 V and 33.2 V) combinations for the up-shifted (2,1) rotating wave at a film thickness of

2.6 nanometers and at an initial frequency splitting of .0053 +/- .0003. In order to evaluate the model, we compare the effects of these parameters to both the data and the model. Toward this end, we may pictorially deconstruct the resonance by focusing on certain features. Three key features include the low amplitude region, the height of the "knee" and the location of the "hook" (see figure 3.2).

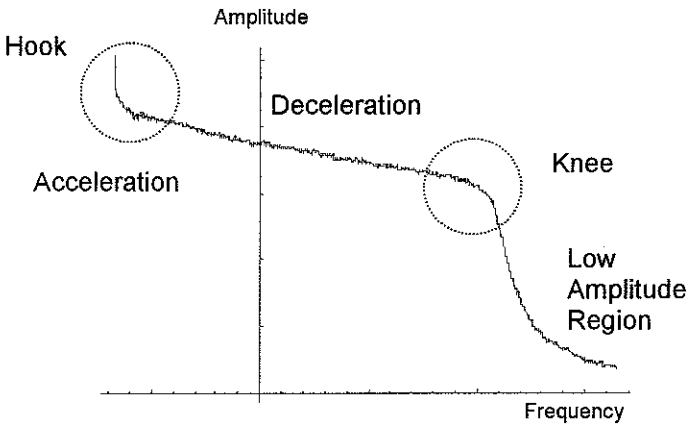

Figure 3.2. Qualitative features of the actual data.

For low to moderate amplitudes, the resonance is well described by the linearized equations of motion and the β-shift. At moderate to high amplitudes, the resonance is characterized by sudden exponential activation of vortices. The deceleration and acceleration regions begin at the "knee" and the "hook", respectively. The data demonstrates a consistent relationship between the initial conditions and these three features, a connection that the model supports.

The height of the "knee", corresponds to a threshold, the minimum wave amplitude and wave velocity necessary to activate vortices. At the "knee" or "hook", the wave and vortex interaction either drives down or drives up the circulation. The below figures illustrate the temperature dependence of the data and the model.

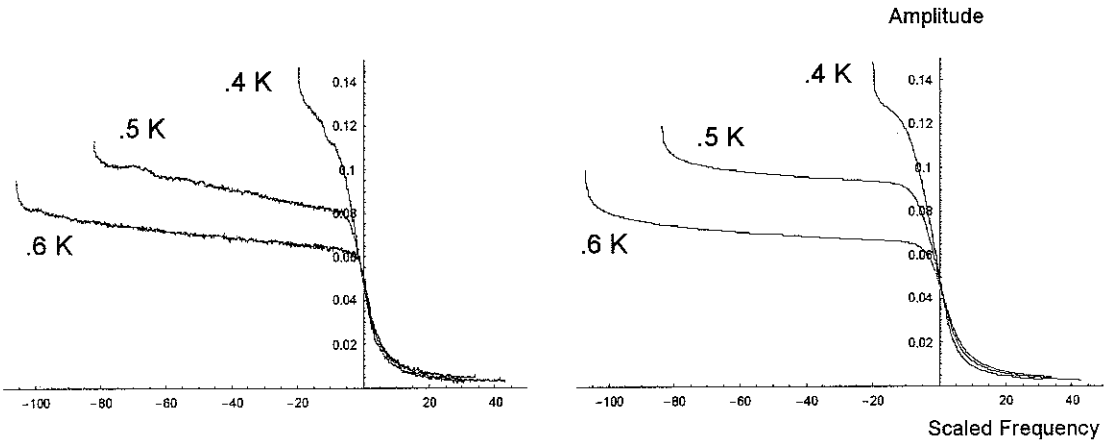

Figure 3.3. The data and model for the 16.5 V drive.

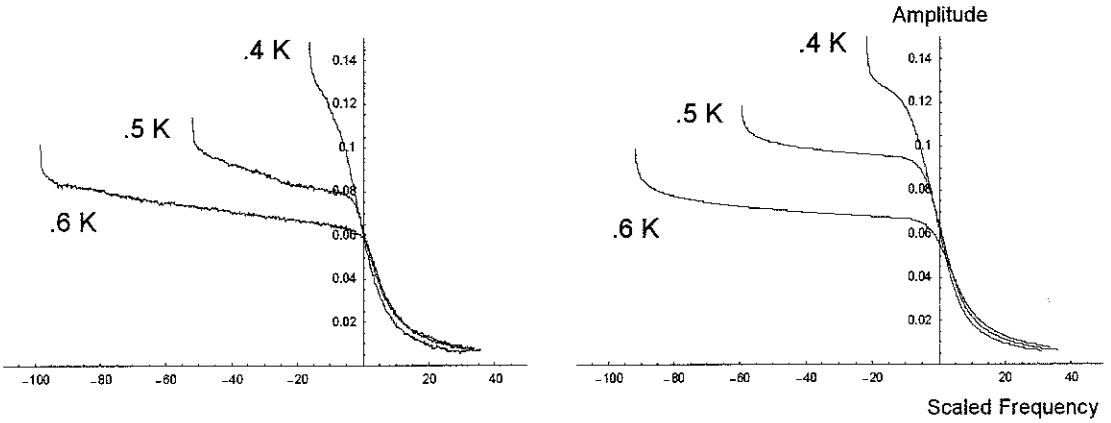

Figure 3.4. The data and model for the 33.2 V drive.

The amplitude is scaled to the film thickness and the frequency is scaled to the quality factor and the initial frequency splitting.

$$amplitude = \frac{\eta_{m,n}}{h_0}$$

$$scaled\ frequency = Q\frac{\Delta f}{f_{center}} \qquad (3.3), (3.4)$$

In figures 3.3 and 3.4, the heights of both the "knee" and the "hook" decrease with increasing temperature. In addition, the "hook" occurs sooner at the lower temperatures and at the bigger drive. This temperature dependence supports the thermal activation model. As the temperature increases, swirling occurs both at smaller circulations and for smaller waves.

The drive voltage effect on the resonance is less intuitive. Big drives are more efficient at driving up the circulation and small drives are more efficient at driving down the circulation.

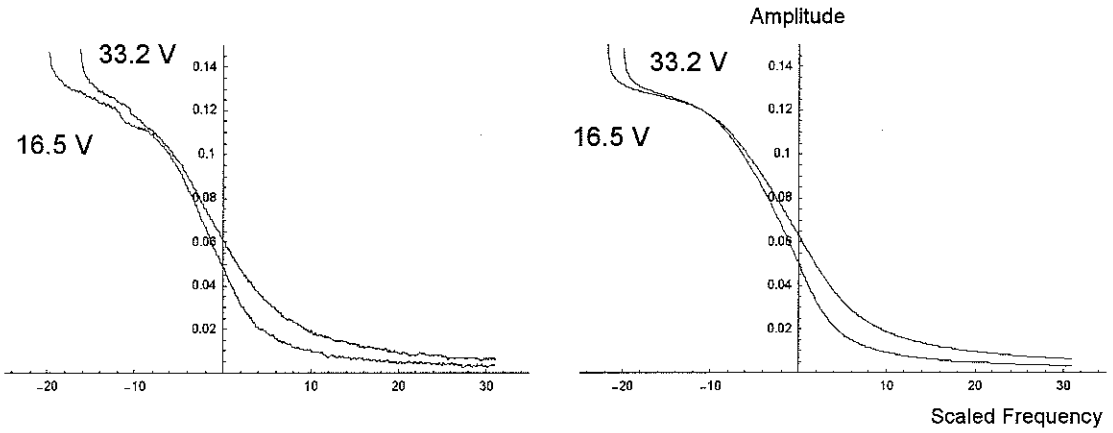

Figure 3.5. The data and model at .4 K.

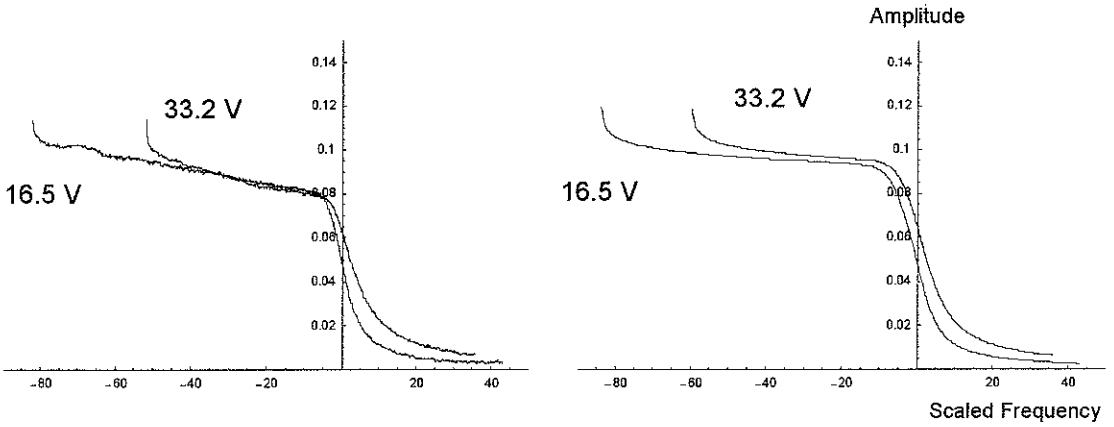

Figure 3.6. The data and model at .5 K.

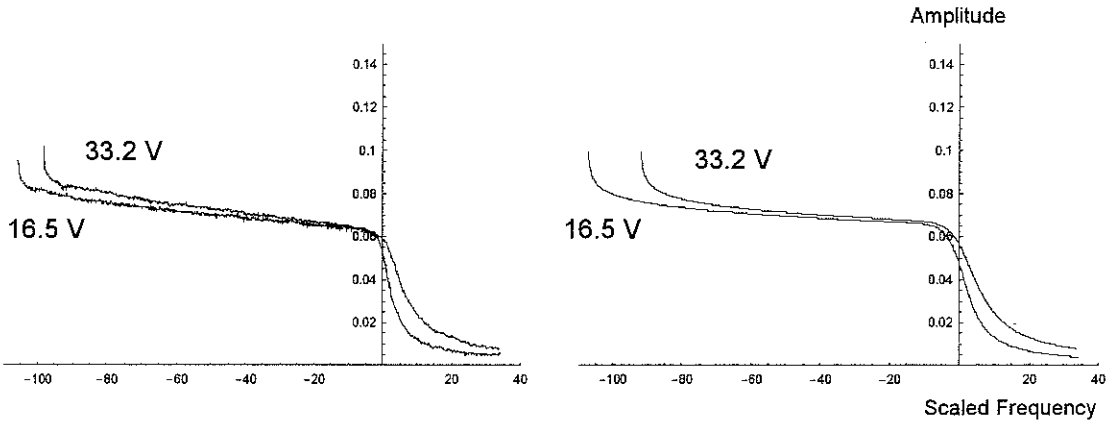

Figure 3.7. The data and model at .6 K.

In the model, large drive amplitudes propel the resonance toward the high amplitude acceleration region faster than small drive amplitudes. A comparison among figures 3.3, 3.4, 3.5, 3.6 and 3.7 indicates that the model matches the general temperature and drive dependence of the data.

Although the model supports the general trends, there are small quantitative discrepancies. These discrepancies include the height of the "knee", location of the "hook" and the slope of the deceleration region.

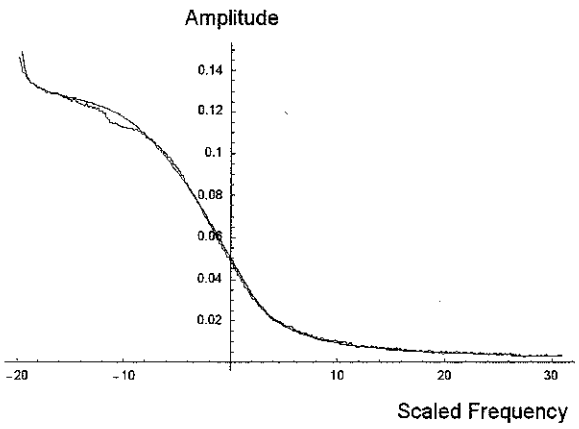

Figure 3.10. .4 K and 16.5 V combination data and model.

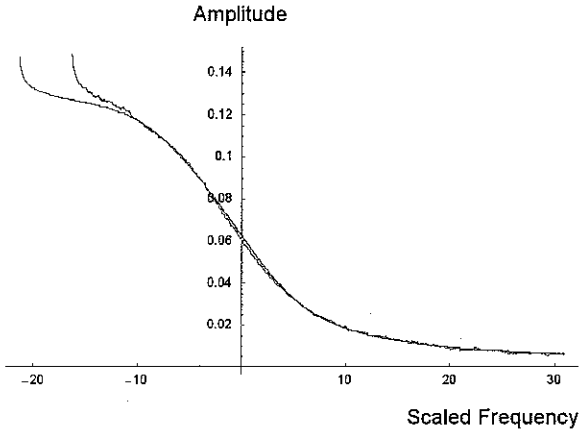

Figure 3.11. .4 K and 33.2 V combination data and model.

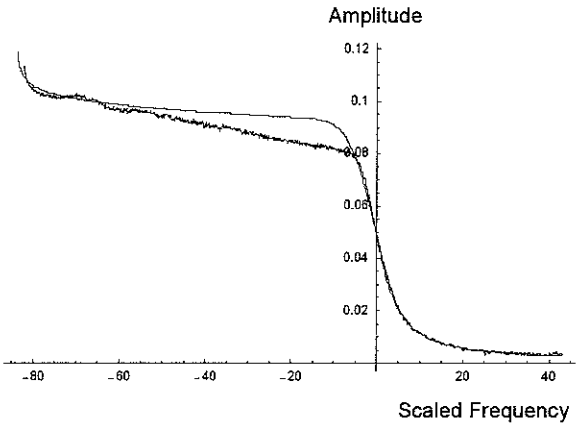

Figure 3.12. .5 K and 16.5 V combination data and model.

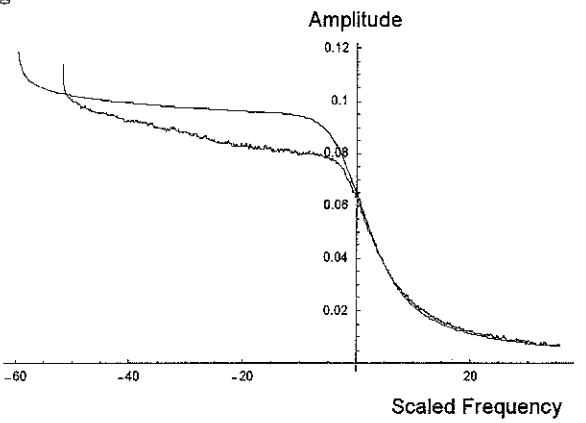

Figure 3.13. .5 K and 33.2 V combination data and model.

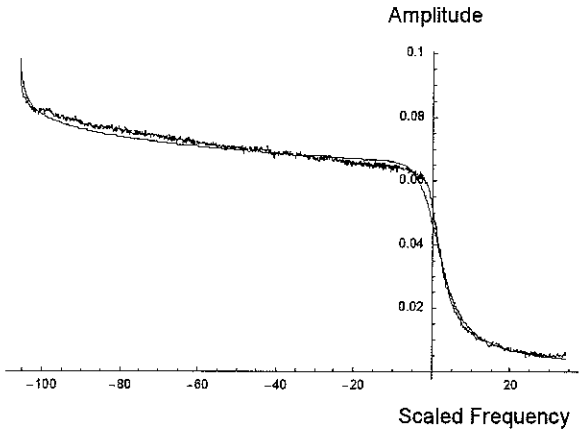

Figure 3.14. .6 K and 16.5 V combination data and model.

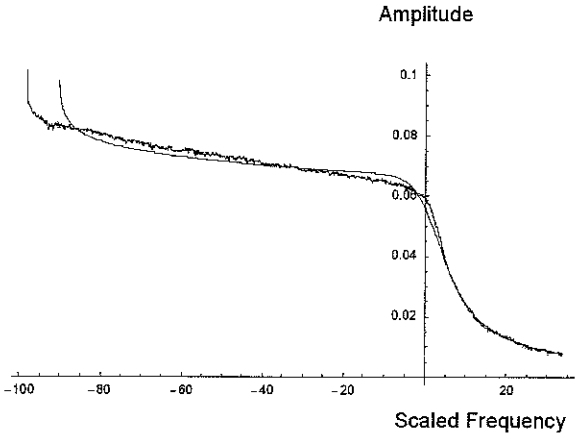

Figure 3.15. .6 K and 33.2 V combination data and model.

In the above plots, the location of the "hook" relative to the model is variable at the higher drive. The fitting routine tends to home in on either the high or low drive data. For the sake of consistency, we arbitrarily give preference to the low drive fit parameters. In the lab, the location of the "hook" is not exactly repeatable. The location may be influenced by the qualitly factor, a value that varies by as much as 20% from one measurement to the next. On the other hand, the height of the "knee" and the slope of the deceleration region is consistently reproducible. The model seems to

give a bigger slope and higher "knee" than the data. Our model for the pinning energy may be over simplified. An exact calculation for the energy levels may be necessary.

3.3 The Numbers

The numerical fits occur in two stages. First the data is truncated at the "knee". In this low amplitude region the background and phase are removed from the data with the appropriate value for η_0 and β. Secondly, the entire resonance is fit to the thermal activation model. Experimentally measured parameters in include the Q and the initial frequency splitting. Adjustable parameters include the characteristic pinning strength (P), the over all scaling factor (R_0), the critical velocity (v_c), the band choice and the weighting factor ($\gamma_{m,n}$) that relates the frequency splitting to the circulation. The band is chosen at the radial coordinate for which the azmuthal wave velocity is a maximum. Here, r_0 is about three quarters the cell radius. The fit is performed simultaneously for all 6 sets of data. Only η_0, β and $\gamma_{m,n}$ are allowed to vary among different data sets.

Remarkably, the Q is constant throughout the resonance. Regardless of nonlinear effects and swirling, the resonance lies on a circle. η_0 is the diameter of this circle. It scales with the square root of the ratio of drive voltages.

$$\eta_{0,high} = (const)\sqrt{\frac{V_{high}}{V_{low}}} \qquad (3.5)$$

The value for β depends upon the initial frequency splitting. The exact relationship is unknown. At very high circulations, β can actually change sign. There are lots of other scans that may quantify the dependence of β on the initial splitting. An analysis could be a topic for future research.

We can directly calculate the weighting factor $\gamma_{m,n}$ from the splittings. However, none are available at the relevent film thickness and temperatures. For this reason, we allow this factor to float. When we change temperatures, the frequency splittings do not change. Initially we did not feel a need to gather this information for every scan. However, if we prepare the film at different temperatures the splittings are different. The preparation involves reseting the circulation to a value close to .005.

The swirling parameters, P, R_0 and v_c, are not independent. Two parameters uniquely determine the other (see Appendix B).

$$R_{combination} = \ln\left(\sqrt{2\pi}R_0\right) - \frac{P}{k_{boltzman}T} \cdot v_{critical} \qquad (3.6)$$

In the numerical analysis, the actual adjustable parameters include a combination scaling factor (R) and the pinning strength (P). A determination of R_0 and $v_{critical}$, require at least two sets of data at different temperatures. The model is weakly sensitive to the characteristic pinning strength. The value is on the order of 50 Kelvin. The over all scaling factor (R_0) is not numerically important. Buried within the factor are several constants of proportionality including a coefficient of friction, a degeneracy factor and so forth. The single most inportant numerical result is the critical velocity. It's value is roughly 4.3 meters per second.

The numerical fits not only provide support for the thermal activation framework but also provide an unbiased and unambiguous value for the critical velocity. Previous measurements are based upon the exponential behavior of swirling as a function of the flow. Generally, critical behavior is not well defined for exponential functions. In this thesis, we define the critical velocity within the framework of the model. It is defined as the minimum external flow necessary to depin a vortex in the absense of thermal activation. Consequently, we are able objectively to compare the critical velocity

among different data sets. The numerical fits to the data show that the critical velocity is independent of the temperature and drive voltage. Further data is required to ascertain the dependence on film thickness and wave mode.

IV

Conclusion

Vortex activation in superfluid films is a complex system and we have chosen a relatively simple model. Regardless, the model matches the general temperature and drive dependence of the data. Our belief in the model provides a basis for defining the critical velocity. Outside the model, the numerical value is not particularly important. However, a comparison of the critical velocity among several sets of data as well as extensions of the model to additional areas of interest will illuminate other characteristics of the general system. These characteristics include the pinning properties and the density of vortices. Further analysis requires additional data at different film thickness and wave modes.

Appendix A

Derivation of the Equations of Motion

If we assume that the fluid is incompressible, the divergence of the fluid velocity must be zero. In cylindrical coordinates, let's separate the parallel and perpendicular components.

$$\vec{\nabla} \cdot \vec{v} = \vec{\nabla}_{//} \cdot \vec{v}_{//} + \frac{\partial v_z}{\partial z} = 0 \qquad \text{(A.1.1)}$$

Typically, our film thickness is millions of times smaller than the cell diameter. Consequently, our film is essentially two-dimensional. We can average over the film thickness.

$$\vec{\nabla}_{//} \cdot \left\langle \vec{v}_{//} \right\rangle + \frac{v_z(h_0) - v_z(0)}{h_0} = 0 \qquad \text{(A.1.2)}$$

The triangular brackets indicate an integral over the film thickness.

$$\langle v \rangle = \frac{1}{h_0} \int_0^{h_0} \frac{\partial v}{\partial z} dz \qquad \text{(A.1.3)}$$

The boundary conditions require that the vertical component of the velocity is zero at the substrate surface. In addition, the vertical component of the velocity at the top is the height oscillation.

$$v_z(0) = 0$$
$$v_z(h_0) = \frac{\partial \eta}{\partial t} \qquad \text{(A.1.4)}$$

The combination of these equations gives the first equation of motion.

$$\frac{\partial \eta}{\partial t} = h_0 \vec{\nabla}_{//} \cdot \left\langle \vec{v}_{//} \right\rangle \qquad \text{(A.1.5)}$$

This equation states that the height oscillations are due only to motion parallel to the substrate surface. If the wavelength is much greater than the film thickness, then there is a negligible vertical acceleration. Changes in the fluid thickness are a consequence of incompressibility.

The second equation of motion is a linearized form of Euler's equation, analogous to Newton's second law. Without viscosity, the acceleration depends only upon the pressure gradient and the van der Waals force.

$$\frac{\partial \vec{v}}{\partial t} = -\frac{1}{\rho} \vec{\nabla} P - \hat{z} g \qquad \text{(A.1.6)}$$

As before, let's separate the parallel and perpendicular components and then take the average over the film thickness.

$$\frac{\partial\langle v_z\rangle}{\partial t} = -\frac{1}{\rho h_0}\left(P(h_0) - P(0)\right) - g$$
$$\frac{\partial\left\langle \vec{v}_{//}\right\rangle}{\partial t} = -\frac{1}{\rho}\vec{\nabla}_{//}\langle P\rangle \qquad \text{(A.1.7)}$$

For an incompressible fluid, the pressure is given by:

$$P = P_0(r,\phi) - \rho g h \qquad \text{(A.1.8)}$$

where, P_0 is the pressure at the surface. Since our experiment runs in a high vacuum, the pressure must be zero at the fluid surface.

$$P_0(r,\phi) - \rho g(\eta + h_0) = 0 \qquad \text{(A.1.9)}$$

The second equation of motion reduces to:

$$\frac{\partial\left\langle \vec{v}_{//}\right\rangle}{\partial t} = -g\vec{\nabla}\eta \qquad \text{(A.1.10)}$$

Relations (A.1.5) and (A.1.10) are the linearized equations of motion.

Appendix B

The Explicit Model

In the original equations of motion let's introduce a periodic driving force and a damping term. The driving force comes from the electrostatic interaction of the capacitor plates and the fluid. For oscillatory motion, a superfluid exhibits energy dissipation. This dissipation is modeled as a simple term, linear in the velocity.

$$\frac{\partial}{\partial t}\left\langle\left(v_r, v_\phi\right)\right\rangle = -g\vec{\nabla}\eta - \gamma\left\langle\left(v_r, v_\phi\right)\right\rangle + \vec{f}_0 e^{-i\omega t}$$
$$\frac{\partial \eta}{\partial t} = -h_0\vec{\nabla}\cdot\left\langle\left(v_r, v_\phi\right)\right\rangle$$

For plane solutions, these equations become a simple matter of linear algebra.

$$\begin{pmatrix} igk & -i(\omega+\gamma) \\ -i\omega & ikh_0 \end{pmatrix}\begin{pmatrix} \eta \\ v \end{pmatrix} = \begin{pmatrix} f_0 \\ 0 \end{pmatrix}$$

If we solve for the steady-state amplitude, we arrive at relationship similar to a mass on a spring.

$$\eta = \frac{ikh_0 f_0}{\omega^2 - ghk^2 - i\gamma\omega}$$

The resonant frequency and the amplitude on resonance determined by patterning the above relationship along the same lines as that of the simple harmonic oscillator.

$$\frac{\eta}{\eta_{resoant}} = \frac{i}{Q(1-\frac{\omega^2}{\omega_0{}^2})+i\frac{\omega}{\omega_0}}$$

$$\eta_{resonant} = -\frac{khf_0}{\gamma\omega_0}$$

$$\omega_0 = k\sqrt{gh_0}$$

$$Q = \frac{\omega_0}{\gamma}$$

In this form, the steady-state amplitude is identical to that of the mass on a spring.

Near resonance, the drive frequency divided by the resonant frequency is close to 1. Let's expand the denominator and keep only first order terms.

$$\frac{\eta}{\eta_{resonant}} \cong \frac{i}{2Q\left(1-\frac{\omega}{\omega_0}\right)+i} \cong \frac{i}{2Q\left(\frac{f_{resonant}-f}{f_{center}}\right)+i}$$

For the simple harmonic oscillator, the resonance frequency is constant. In our system, this frequency is modified by nonlinearity of the wave and a Doppler effect. Taken together, the resulting equation is given by:

$$f_{resonant} = f_{center}\left(1\pm\gamma_{m,n}\frac{v_{background}(r_0)}{c_3}-\beta\left(\frac{\eta}{h_0}\right)^2\right)$$

To simplify matters, let's define several new variables.

$$f_{swirl} = f_{center}\left(1\pm\gamma_{m,n}\frac{v_{background}(r_0)}{c_3}\right)$$

The swirl frequency is the low amplitude resonant frequency that we physically measure in the lab. The scaled frequencies are given by:

$$X = Q\frac{f_{driv} - f_{swirl}}{f_{center}}$$

$$X_r = Q\frac{f_{resonant} - f_{swirl}}{f_{center}} = -B\left(\frac{\eta}{h_0}\right)^2$$

Here, the product of β and Q is defined a B. The resonant frequency may be solved for as the solution to the cubic.

$$X_r^{\,3} + (-2X)X_r^{\,2} + \frac{1+4X^2}{4}X_r + B = 0$$

This equation is the combination of the steady-state amplitude and the frequency shifts. The resonance may now be written in its most useful and final form.

$$\frac{\eta}{\eta_{resonant}} = \frac{1}{2(X_r(r,\phi) - X) - i}$$

The next section deals with the acceleration of the background circulation. This calculation requires an integral that cannot be computed in closed form.

$$a(\eta_{m,n}, v_{background}) = \frac{\partial v_{background}}{\partial t} = -\int_0^{2\pi} R_0 v_{\sup erfluid} e^{\frac{P(|v_{\sup erfluid}| - v_{critical})}{k_{boltzman}T}} d\theta$$

Numerical integration techniques are too slow and a gaussian approximation has been made. The wave velocity is be expanded to second order. Thereby, the integral may be solved analytically.

$$a(\eta_0, v_b) =$$

$$-e^R \sqrt{\frac{x_0}{\varepsilon \cdot m \cdot \eta_{m,n}}} \left((1+\eta_0) \left(v_b + \frac{v_p}{1+\eta_0} - \frac{1}{2\varepsilon} \right) e^{\varepsilon \left(v_b + \frac{v_p}{1+\eta_0} \right)} + (1-\eta_0) \left(v_b - \frac{v_p}{1-\eta_0} + \frac{1}{2\varepsilon} \right) e^{\varepsilon \left(-v_b + \frac{v_p}{1-\eta_0} \right)} \right)$$

where,

$$x_0 = \frac{x_{m,n} r_0}{a}$$

$$\eta_0 = \eta_{m,n} J_m(x_0)$$

$$v_p = c_3 \frac{\eta_{m,n}}{h_0} \frac{m}{x_0} J_m(x_0)$$

$$\varepsilon = \frac{P}{k_{boltzman} T}$$

The most important relationship is given by the following.

$$R = \ln\left(\sqrt{2\pi} R_0\right) - \varepsilon \cdot v_{critical}$$

R and ε are two of the fit parameters. The critical velocity is calculated as the slope.

Bibliography

Ellis, F. M. and Zimmermann, C. L., *J. Low Temp Phys.*, **101**, 475 (1995)

Baierlein, Ralph, Ellis, F. M., and Luo, Hai, *J. Low Temp Phys.*, **108**, 31 (1997)

Tilley, D. R. and Tilley, J., Superfluidity and Superconductivity (Halsted Press, New York, 1974)

Luo, Hai, Ph. D. thesis, (Wesleyan University, 1992)

Wilson, C. L., Ph. D. thesis (Wesleyan University, 1992)

Ellis, F. M. and Li, L., *Phys. Rev. Lett.*, **71**, 1577 (1993)

Wilson, C. L. and F. M. Ellis, *J. Low Temp Phys.*, **101**, 507 (1995)

Ellis, F. M. and Wilson, C. L., *J. Low Temp Phys.*, **113**, 411 (1998)

Missing:

Hydrodynamics, Lamb.

Thermal Physics, Baierlein.